RADIATION OF VERTICAL DIPOLE ANTENNAS OVER FLAT AND LOSSY TERRAIN : A NOVEL EFFICIENT METHOD FOR THE ACCURATE NUMERICAL CALCULATION OF THE SOMMERFELD INTEGRALS IN THE SPECTRAL DOMAIN

S. Bourgiotis[1], L. Dimopoulos[1], Th. Lymperopoulos[1], A.Chrysostomou[1], S. Sautbekov[2], and P. Frangos[1]

[1]*School of Electrical and Computer Engineering,*

National Technical University of Athens,

9, Iroon Polytechniou Str., 157 73, Zografou, Athens, Greece

Tel. +30 210 772 3694, Fax. +30 210 772 2281, E-mail : pfrangos@central.ntua.gr

[2] *Al-Farabi Kazakh National University, Department of Physics, Almaty, Kazakshtan*

E-mail : sautbek@mail.ru

Abstract

In this paper, the integral expressions of the well-known 'Sommerfeld Radiation Problem', derived by our research group entirely in the spectral domain – as opposed to most classical formulations – are re-evaluated. Numerical integration has revealed various disadvantages regarding the accuracy as well as convergence times of existing formulas. This resulted in their limited practical validity, constrained in the low frequency regime. However, through a proper variable transformation it is possible to convert them into more compact formulas, which overcome the flaws of previous expressions. As a result, convergence times are significantly reduced and, even more important, the new expressions allow for the calculation of the total received EM field of a radiating dipole above flat lossy ground, at almost an arbitrarily chosen level of accuracy. Simulation results, presented herein, indicate the effectiveness and correctness of the proposed method, which can be easily implemented in a general – purpose computer code platform.

1. Introduction

The 'Sommerfeld radiation problem' is a well-known problem in the area of propagation of electromagnetic (EM) waves above flat and lossy ground [1]. The original Sommerfeld solution to this problem is provided in the physical space by using the 'Hertz potentials' [1]. An equivalent solution to the problem is achieved by working in the spectral domain. In that perspective, in [2] the authors derived simple 1-D integral expressions for the received EM field, which compared to the classical Sommerfeld formulation, do not require taking the potential's derivative, in order to calculate the received field. They also allow the application of asymptotic techniques, like the Stationary Phase Method [3], leading to well-known analytic formulas, applicable in the high frequency regime.

However, accurately evaluating Sommerfeld integrals is not a trivial task. Particularly, it is true that the integral expressions of [2] are generalized integrals, extending from minus infinite to plus infinite and with the integrands presenting singularities, along the integration path. For that reason, the residue theory, along with approximation techniques like the method of Saddle Points, is so widely used by most researchers in the literature in their attempt to evaluate Sommerfeld integrals [4], [5]. However, there is always an accuracy issue that arises when a pole point resides close to the path of integration and even evaluating those integrals purely numerically, required expensive commercial software [5].

In this paper we show that using an appropriate variable transformation it is possible to convert the generalized integrals of [2] into fast converging formulas. Particularly, the integral expression describing the received EM field, is broken down into two parts, one easily computed definite integral and an integral of semi-infinite range. However, the integrand of this second generalized integral, becomes a fast decaying exponential function, resulting in very fast convergence times.

Simulations and comparisons with known literature results [6] are given. Moreover, comparing the new results, with those obtained in [7], which refer to the evaluation of the original integral expressions of [2], without performing the variable transformation, introduced in this paper, indicate the accuracy and the effectiveness of the method.

2. Problem Geometry

The problem geometry is shown in Fig. 1 and described extensively in [1], [2], [4 – 7]. In summary, *p* represents the dipole moment of a radiating vertical Hertzian Dipole at frequency *f*, located at altitude x_0, above infinite, flat and lossy ground, σ being its ground conductivity. Here (ε_1,μ_1), (ε_2,μ_2) represent the constitutive parameters of the air and ground respectively, with ε_0=8,854x10^{-12}F/m being the absolute permittivity in vacuum or air.

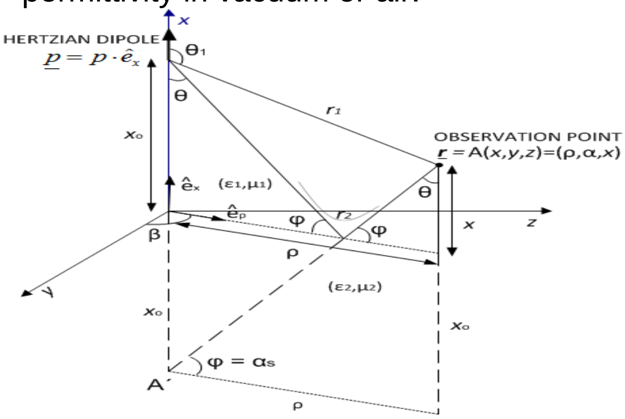

Figure 1. Geometry of the problem

3. Disadvantages concerning the Numerical Integration of the original Spectral Domain Representation for the Received EM Field

In [2], [4] it is shown that the scattered electric field at the receiver's position, above the ground level (x>0) can be expressed by:

$$\underline{E}^R = -\frac{ip}{8\pi\varepsilon_0\varepsilon_1}\int_{-\infty}^{+\infty}\underline{\mathrm{f}}(k_\rho)dk_\rho \qquad (1)$$

where:

$$\underline{\mathrm{f}}(k_\rho) = \left(\kappa_1\hat{\mathrm{e}}_\rho - \left|k_\rho\right|\hat{\mathrm{e}}_x\right) k_\rho \left|k_\rho\right| \cdot$$
$$\cdot\frac{\varepsilon_2\kappa_1 - \varepsilon_1\kappa_2}{\kappa_1\left(\varepsilon_2\kappa_1 + \varepsilon_1\kappa_2\right)}\mathrm{H}_0^{(1)}\left(k_\rho\rho\right)e^{i\,\kappa_1(x+x_0)} \qquad (2)$$

and:

$$\kappa_1 = \sqrt{k_{01}^2 - k_\rho^2}\,,\ \kappa_2 = \sqrt{k_{02}^2 - k_\rho^2} \qquad (3)$$

In (2), (3) $\mathrm{H}_0^{(1)}$ is the Hankel function of first kind and zero order and k_{01}, k_{02} the wavenumbers of propagation in the air and lossy ground respectively.

Expressions (1) – (3) expose the following difficulties when coming to numerically evaluate the respective integral:

- The range of integration extends from $-\infty$ to $+\infty$, resulting in potential errors for large evaluation arguments, despite the fact that the phase factor of (2), i.e. $e^{i\,\kappa_1(x+x_0)}$ gets exponential decaying with respect to k_ρ.
- The Hankel function exhibits a singularity at $k_\rho = 0$ and although it is proved that this singularity does not break the integral's convergence [7], it can affect the accuracy of the numerical integration results, when implemented in the computer.
- As seen from (2), $k_\rho = k_{01}$ is another singularity of the integrand and consequently a sufficient small range around it must be excluded when numerically evaluating (1). As mentioned in [7], doing so may severely affect the accuracy of the results.

4. Re-formulating the integral representation for the EM field

Eq. (1) may be written as:

$$\underline{E}^R = -\frac{ip}{8\pi\varepsilon_0\varepsilon_1}(I_1 + I_2 + I_3) \qquad (4)$$

where,
$$\begin{cases} I_1 = \displaystyle\int_{-k_{01}}^{+k_{01}}\underline{\mathrm{f}}(k_\rho)dk_\rho & (5a) \\ I_2 = \displaystyle\int_{k_{01}}^{+\infty}\underline{\mathrm{f}}(k_\rho)dk_\rho & (5b) \\ I_3 = \displaystyle\int_{-\infty}^{-k_{01}}\underline{\mathrm{f}}(k_\rho)dk_\rho & (5c) \end{cases}$$

For I_1, we perform the following variable transformation: $k_\rho = k_{01}\sin\alpha$, which obviously maps the $[-k_{01},\ +k_{01}]$ range in the k_ρ domain to [-π/2 , π/2] of angle α. With this transform it also holds true:

$$\kappa_1 = k_{01}\cos\alpha,\ \kappa_2 = \sqrt{k_{02}^2 - k_{01}^2\sin^2\alpha} \quad (6)$$

Applying the above mentioned variable transform to (5a) and with the use of (2),(6), the expression for I_1 becomes:

$$I_1 = k_{01}^3 \int_{-\pi/2}^{+\pi/2} \begin{array}{l} \left(\cos\alpha\,\hat{e}_\rho - \left|\sin\alpha\right|\,\hat{e}_x\right)\sin\alpha\,\left|\sin\alpha\right|\cdot \\ R_{\|}(\alpha)\cdot H_0^{(1)}\left(\rho\,k_{01}\sin\alpha\right)e^{i\,k_{01}(x+x_0)\cos\alpha}\,d\alpha \end{array} \quad (7)$$

with:

$$R_{\|}(\alpha) = \frac{\varepsilon_2 k_{01}\cos\alpha - \varepsilon_1\sqrt{k_{02}^2 - k_{01}^2\ \sin^2\alpha}}{\varepsilon_2 k_{01}\cos\alpha + \varepsilon_1\sqrt{k_{02}^2 - k_{01}^2\ \sin^2\alpha}} \quad (8)$$

Expression (7) may be further broken down into two integrals:

$$I_1 = k_{01}^3 \left\{ \begin{array}{l} \displaystyle\int_0^{+\pi/2} \left[\begin{array}{l} \left(\cos\alpha\,\hat{e}_\rho - \sin\alpha\,\hat{e}_x\right)\ \sin^2\alpha\cdot R_{\|}(\alpha)\cdot \\ H_0^{(1)}\left(\rho\,k_{01}\sin\alpha\right)e^{ik_{01}(x+x_0)\cos\alpha} \end{array} \right]\cdot d\alpha - \\ \displaystyle -\int_{-\pi/2}^{0} \left[\begin{array}{l} \left(\cos\alpha\,\hat{e}_\rho + \sin\alpha\,\hat{e}_x\right)\ \sin^2\alpha\cdot R_{\|}(\alpha)\cdot \\ H_0^{(1)}\left(\rho\,k_{01}\sin\alpha\right)e^{ik_{01}(x+x_0)\cos\alpha} \end{array} \right]\cdot d\alpha \end{array} \right\}$$

Finally, observing from (8) that $R_{\|}(-\alpha) = R_{\|}(\alpha)$ and using the properties of the Hankel function:

$$H_0^{(1)}(z) + H_0^{(2)}(z) = 2J_0(z) \quad (9)$$

$$H_0^{(1)}(z\cdot e^{i\pi}) = -H_0^{(2)}(z) \quad (10)$$

it is easy to show that:

$$I_1 = 2\,k_{01}^3 \int_0^{\pi/2} \left[\begin{array}{l} \left(\cos\alpha\,\hat{e}_\rho - \sin\alpha\,\hat{e}_x\right)\cdot\ \sin^2\alpha\cdot R_{\|}(\alpha)\cdot \\ J_0\left(\rho\,k_{01}\sin\alpha\right)\ \cdot\ e^{i\,k_{01}(x+x_0)\cos\alpha} \end{array} \right] d\alpha \quad (11)$$

with J_0 being the zero order Bessel function.

For I_2 and I_3, a similar approach is followed. This time the variable transformations, $k_\rho = k_{01}\cosh\alpha$ and $k_\rho = -k_{01}\cosh\alpha$ are used respectively, which both map the original ranges of integration in k_ρ, i.e. $[k_{01},\ +\infty]$ and $[-\infty, -k_{01}]$ to $[0,\ +\infty]$ of variable α. Moreover, in both cases:

$$\kappa_1 = ik_{01}\sinh\alpha,\ \kappa_2 = \sqrt{k_{02}^2 - k_{01}^2\cosh^2\alpha} \quad (12)$$

Consequently, applying a similar reasoning, as with I_1 and also using (9), (10), it is easy to combine the results for I_2 and I_3 as following:

$$I_2 + I_3 = \frac{2k_{01}^3}{i}\int_0^{\infty} \left[\begin{array}{l} \left(i\sinh\alpha\,\hat{e}_\rho - \cosh\alpha\,\hat{e}_x\right)\cdot\cosh^2\alpha\cdot \\ R_{\|}'(\alpha)\cdot J_0\left(\rho\,k_{01}\cosh\alpha\right)\cdot e^{-k_{01}(x+x_0)\sinh\alpha} \end{array} \right] d\alpha \quad (13)$$

where :

$$R_{\|}'(\alpha) = \frac{i\varepsilon_2 k_{01}\sinh\alpha - \varepsilon_1\sqrt{k_{02}^2 - k_{01}^2\ \cosh^2\alpha}}{i\varepsilon_2 k_{01}\sinh\alpha + \varepsilon_1\sqrt{k_{02}^2 - k_{01}^2\ \cosh^2\alpha}} \quad (14)$$

From (4), (11), (13), the expression for the scattered electric field becomes :

$$\underline{E}^R = -\frac{ipk_{01}^3}{4\pi\varepsilon_0\varepsilon_1} \left\{ \begin{array}{l} \displaystyle\int_0^{\pi/2} \left[\begin{array}{l} \left(\cos\alpha\,\hat{e}_\rho - \sin\alpha\,\hat{e}_x\right)\cdot\ \sin^2\alpha\cdot \\ R_{\|}(\alpha)\cdot J_0\left(\rho\,k_{01}\sin\alpha\right)\cdot e^{i\,k_{01}(x+x_0)\cos\alpha} \end{array} \right] d\alpha - \\ \displaystyle -i\int_0^{\infty} \left[\begin{array}{l} \left(i\sinh\alpha\,\hat{e}_\rho - \cosh\alpha\,\hat{e}_x\right)\cdot\cosh^2\alpha\cdot \\ R_{\|}'(\alpha)\cdot J_0\left(\rho\,k_{01}\cosh\alpha\right)\cdot e^{-k_{01}(x+x_0)\sinh\alpha} \end{array} \right] d\alpha \end{array} \right\}$$

(15)

5. Comparisons – Numerical Results

The new integral form, given by (15), facilitates the numerical evaluation of the EM field, since it overcomes the major drawbacks of expressions (1) – (3), outlined in section 3. Particularly:

- The Hankel function, $H_0^{(1)}$, is substituted by the zero order Bessel function, J_0 ,which has no singularity, whatsoever.
- The integrand has no singularity at $k_\rho = k_{01}$, hence no need to exclude any range around k_{01} is required.
- The result is expressed as the sum of two integrals, one bound definite integral, ranging from [0, π/2] and an improper integral extending from $[0,\ +\infty]$. However, due to the

presence of $e^{-k_{01}(x+x_0)\sinh\xi}$, the second integrand is a fast decaying function, practically making the integral a bound limits one that is fast converging and easily evaluated in the computer.

The above justifications are validated by simulation results.

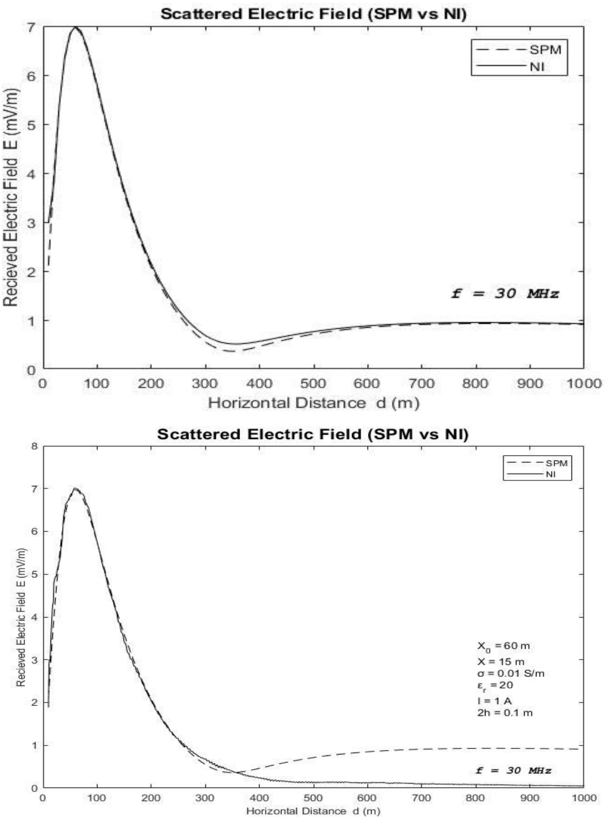

Figure 2. Comparison of Numerical Integration results for the scattered field using : (i) redefined integral expressions (upper figure), (ii) earlier derived spectra integral expressions (lower figure)

The top graph of Fig. 2 depicts the numerical evaluation for the scattered electric field, using (15). It is compared (bottom graph) against the equivalent results of [7], in which the computation was based on the original integral form, given by (1) – (3). In both cases, numerical integration (NI) data are represented by the solid lines of Fig. 2. The parameters for the simulation (i.e. transmitter – receiver heights, ground parameters, operating freq. etc) are given in the bottom plot of Fig.2.

Along with the NI results, the high frequency approximation data, obtained after the application of the SPM method to the integral expressions for the Electric field [2], are shown as well (dashed lines). As mentioned in [7], SPM formulas are expected to be accurate in the far field, i.e. at least at distances over 10 – 15 wavelengths, or above 100 – 150m, for the 30MHz case and the problem parameters shown in Fig. 2. Therefore, using the SPM data as the baseline, it is obvious that only the numerical evaluation of (15) achieves the required accuracy. On the contrary, numerical computation of (1) – (3) fails to describe the electric field and this may be attributed to the reasons analyzed in Section 3 above.

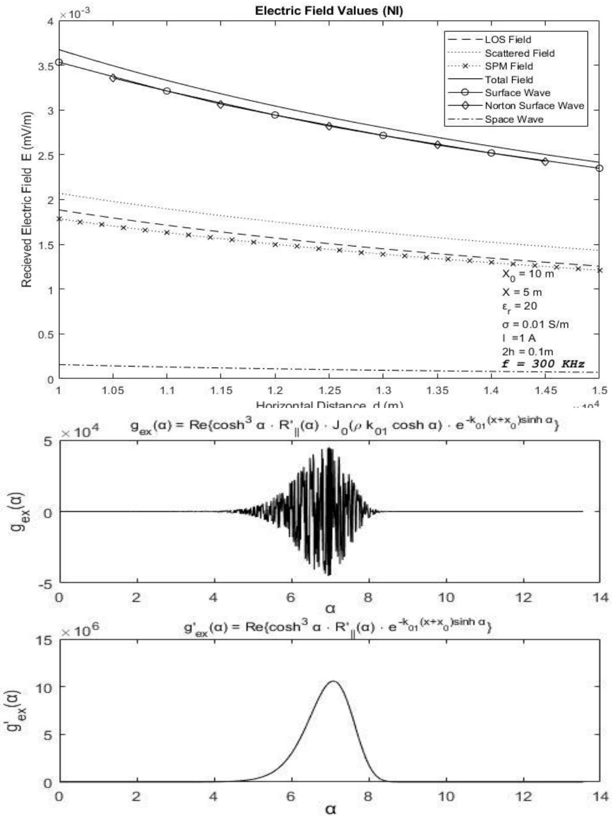

Figure 3. Numerical evaluation of the EM field at the '*<u>low Frequency regime</u>*'

In Fig. 3 (top graph), the components of the total received field, for a *Low Frequency (LF) scenario*, are shown. For the direct (LOS) field and the Space Wave, analytic formulas exist, as used in [7]. The scattered field was numerically computed via (15).

Due to the small antenna heights and the long distances involved (~10km), the space wave is expected to diminish [3]. As a result, the link is established primarily by means of the Surface Wave, which is defined as the remaining field, after subtracting the space wave from the total field [5]. This is actually verified in Fig. 3, with the Total Field curve being very close to the Surface Wave results. As a confirmation of the validity of the results, our Surface Wave calculations are compared with the respective Norton formulas [6]. The respective curves are almost identical!

The bottom half of Fig. 3 displays the behavior of the integrand, $g_{ex}(\alpha)$ (actually the real part of the x-directed component), of the second integral expression of (15). It is evident that this integrand is confined in a small window of the integration variable α, outside of which and especially for large values of α, it actually becomes equal to zero. This is attributed to the behavior of the exponential function of the integrand, $e^{-k_{01}(x+x_0)\sinh\alpha}$. Due to the presence of the sinh function in the exponent, it is a vastly decreasing factor, making the whole integrand almost zero for even modest values of α. The bottom line is that the generalized integral of (15) becomes a practically bound limits one, easily and quickly evaluated in the computer.

The oscillations in $g_{ex}(\alpha)$ originate from the behavior of the Bessel function J_0. Its effects on the integrand are visible by comparing the two bottom graphs of Fig. 3. Due to these oscillations, most of the effect of $g_{ex}(\alpha)$ is cancelled, which is why the relative large values of $g_{ex}(\alpha)$ (~10^4) are not reflected in the final field values (~10^{-5})

The simulation of Fig. 3 is now repeated at Fig. 4 for a *high frequency scenario* in the VHF/UHF band. Again, the source and observation points are located close to the ground level and the electric field values at various distant observation points are calculated.

As shown in Fig. 4, in this case the observed Surface Wave is negligible, a result also predicted by Norton [6]. Consequently, the Space Wave almost completely describes the total received field and hence the SPM method, an asymptotic method that converges to the space wave formulas [2], [7], is validated in this high frequency case, despite the small grazing angle (angle φ of Fig. 1) of the scenario [7]. Finally, notice in the bottom graph of Fig. 4 how quickly, $g_{ex}(\alpha)$ vanishes, making thus the convergence of (15) very fast.

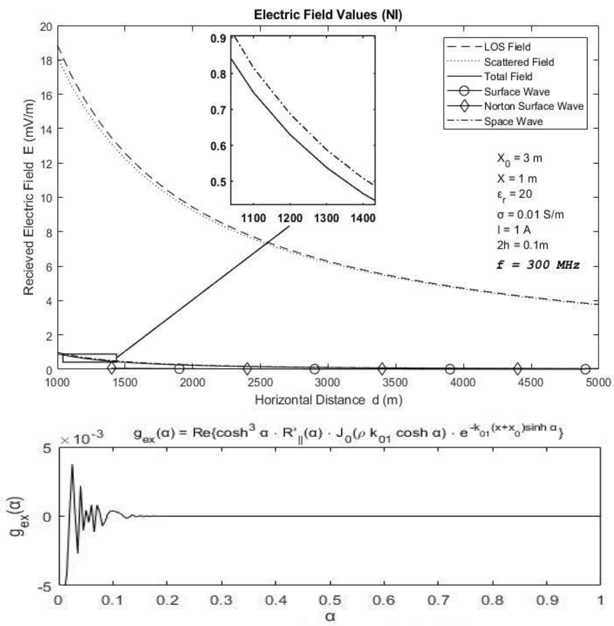

Figure 4. Numerical evaluation of the EM field at the VHF/UHF band (<u>'high frequency regime'</u>)

As a final validation, the field values (*this time for the magnetic field*) for the scenario of Fig. 2 (i.e. frequency f=30 MHz) are shown in Fig. 5. Again, it seems there is a very good match between our calculations with the respective Norton's results [6].

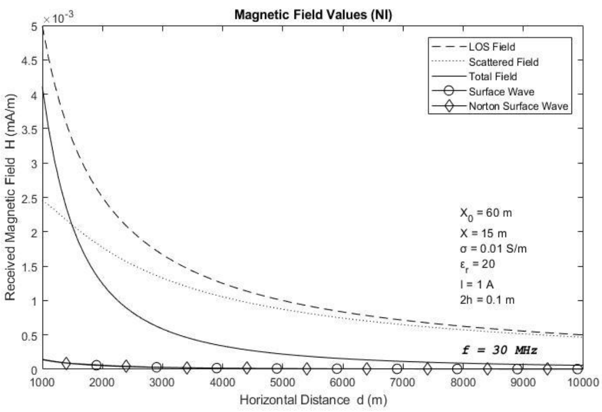

Figure 5. Magnetic field components at the frequency of 30MHz

4. Conclusion

In this paper we continue our previous research work on the solution of the 'Sommerfeld radiation problem' in the spectral domain. Using an appropriate variable transformation, it is shown that the disadvantages of the previous integral expressions for the EM field are effectively addressed. The EM field is now expressed as an integral formula, which is easy and fast to evaluate in the computer, using a general purpose computer code suite, as opposed to commercially specialized software, used in the literature [5].

Details about the algorithm, used and the specifics of the implementation code will be given in the accompanying Journal paper, currently prepared by our research team. For the time it is enough to say that the results, presented herein, were obtained with a required relative accuracy level of 10^{-3}, although in most of the cases the achieved, estimated accuracy was less than 10^{-5} (meaning that the algorithm might accept further improvements for even faster computation times). With this setting, only a few seconds or even parts of a second (depending on the case) were just enough to estimate the EM field, at each reception point (horizontal distance from the source). Higher accuracy levels are addressable by the algorithm (e.g. the algorithm was run with a 10^{-10} setting) requiring, however, larger convergence times. Nevertheless, from a visualization perspective, the captured graphs differed imperceptibly from the ones shown here.

References

[1] A. N. Sommerfeld, "Propagation of Waves in Wireless Telegraphy", Ann. Phys., 28, pp. 665–736, March 1909; and 81, pp. 1135–1153, December 1926.

[2] K. Ioannidi, Ch. Christakis, S. Sautbekov, P. Frangos and S.K. Atanov, "The radiation problem from a vertical Hertzian dipole antenna above flat and lossy ground: novel formulation in the spectral domain with closed-form analytical solution in the high frequency regime", *International Journal Antennas and Propagation*, Hindawi Ed. Co., Special Issue 'Propagation of electromagnetic (EM) waves over terrain' (PEWT), vol. 2014.

[3] C. A. Balanis, Antenna Theory: Analysis and Design, New York: J. Wiley and Sons Inc., 1997, Appendix VIII: Method of Stationary Phase, pp. 922–927.

[4] Seil Sautbekov, Sotiris Bourgiotis, Ariadni Chrysostomou and Panayiotis Frangos, 'A Novel Asymptotic Solution to the Sommerfeld Radiation Problem: Analytic field expressions and the emergence of the Surface Waves', 'Progress in Electromagnetics Research M' Journal ('PIER M'), Vol. 64, pp. 9-22, 2018.

[5] T. K. Sarkar et. al., "Electromagnetic Macro Modelling of Propagation in Mobile Wireless Communication: Theory and Experiment", *IEEE Antennas and Propagation Magazine*, Vol. 54, No. 6, pp. 17–43, Dec. 2012.

[6] K. A. Norton, "The Propagation of Radio Waves Over the Surface of the Earth", Proceedings of the IRE, 24, pp. 1367–1387, 1936; and 25, pp. 1203–1236, 1937.

[7] A. Chrysostomou et. al., "Radiation of a Vertical Dipole Antenna over Flat and Lossy Ground: Accurate Electromagnetic Field Calculation using the Spectral Domain Approach along with Redefined Integral Representations and corresponding Novel Analytical Solution", *Electronics and Electrical Engineering Journal*, Vol. 22, No. 2, 2016.